http://dx.doi.org/10.5012/bkcs.2012.33.9.3043

Light Scattering Amplification on Dye Sensitized Solar Cells Assembled by Hollyhock-shaped CdS-TiO_2 Composites

Gayoung Lee, Huryul Lee, Myeong-Heon Um,† and Misook Kang*

Department of Chemistry, College of Science, Yeungnam University, Gyeongsan, Gyeongbuk 712-749, Korea
**E-mail: mskang@ynu.ac.kr*
†Department of Chemical Engineering, College of Engineering, Kongju National University, Cheonan, Chungnam 330-717, Korea
Received May 14, 2012, Accepted June 19, 2012

To investigate the scattering layer effect of a TiO_2 multilayer in dye-sensitized solar cells (DSSCs), we designed a new DSSC system, assembled with a CdS-TiO_2 scattering layer electrode. A high-magnification SEM image exhibited hollyhock-like particles with a width of 1.5-2.0 μm that were aggregated into 10-nm clumps in a hexagonal petal shape. The efficiency was higher in the DSSC assembled with a CdS-TiO_2 scattering layer than in the DSSC assembled with TiO_2-only layers, due to the decreased resistance in electrochemical impedance spectroscopy (EIS). The short-circuit current density (J_{sc}) was increased by approximately 7.26% and the open-circuit voltage (V_{oc}) by 2.44% over the 1.0 wt % CdS-TiO_2 composite scattering layer and the incident photon-to-current conversion efficiency (IPCE) in the maximum peak was also enhanced by about 5.0%, compared to the DSSC assembled without the CdS-TiO_2 scattering layer.

Key Words : Dye-sensitized solar cells, CdS-TiO_2, Scattering layer, Incident photon-to-current conversion efficiency, Electrochemical impedance spectroscopy

Introduction

In recent years quantum-confined semiconductor nanoparticles such as CdS and CdSe which are important group II-VI semiconductors have attracted considerable attention due to their unique size-dependent chemical properties connecting with their potential applications in light-emitting diodes, optoelectronic devices and even photocatalysis.[1-10] To date, great efforts have been focused on the design of effective methods to synthesize nanostructure such as nanowires, nanobelts and nanotubes due to the unique properties of these structures. Many synthetic methods have been employed to prepare CdS nanoparticles, including soft chemical reaction, solid-state reaction, sol-gel process, spray-pyrolysis methods, sono-chemical preparation, microwave-heated method, and PVP-assisted solvothermal method.[1-4] However, the application at the turn of last is getting rather wider because its band gap (2.3 eV) corresponds well with the spectrum of visible sunlight. A typical example is utilized as the photosensitizer in solar cells.[11-14] Zhou *et al.*[12] reported that CdS-sensitized branched TiO_2 multi-sized nanorod film electrode had a better solar cell performance with a high open-circuit voltage (V_{oc}) of 0.68 V, a short-circuit current density (J_{sc}) of 2.53 mA/cm^2 and a conversion efficiency of 0.71%. And Chen *et al.* suggested[13] that the performance could be improved by optimizing the CdS nanorod structure and the structural regularity, or by choosing more efficiently interfacial ligand molecules. However, when used as a photosensitizer, the poor efficiency necessitates considerable advances before commercialization can be achieved, and access to new CdS applications is required.

The optimized electrode consists of spherical particles of 10-20 nm diameter with high surface area and a thickness of about 10-14 μm. The electrodes are formed by two methods: two layers of TiO_2 of the same size are used, and particles of different sizes are used to make two layers of TiO_2. The TiO_2 particles typically used in dye-sensitized solar cells (DSSCs) have a diameter of approximately 20 nm, through which it is easy for long wavelengths of light to permeate, but because the long-wavelength light in solar cells is not used effectively there have been few gains in efficiency. In recent years, DSSCs assembled with the second film consisting of a 4-5 μm thick layer made from large nanoparticles or nanopores coated on the top of dense TiO_2 electrodes have exhibited increased efficiency.[15] The added second layer consisting of a TiO_2 layer of 400 nm size acts as the scattering material for increasing the incident light path, resulting in an array of more photons that can be obtained to improve the current density.[16] This confirmed the importance of the scattering materials in DSSC assembly. A combination of nano-structured TiO_2 and CdS electrodes in DSSCs was investigated in this study in order to improve the light-efficiency of solar cells. Based on the scattering effect on the CdS-TiO_2 composites, the optical properties of the appropriate cells with the highest efficiency were determined.

Experimental Section

Synthesis and Characteristics of CdS. CdS was prepared using a conventional hydrothermal treatment as described in the literature.[1-10] To prepare the sol mixture, sodium sulfate ($Na_2S_2O_3 \cdot 5H_2O$ 99.9%, Junsei Chemical, Japan) and cadmium chloride ($Cd(Cl)_3 \cdot 2.5H_2O$, 99.9%, Junsei Chemical, Japan) were used as the S and Cd precursors, respectively.

Cadmium chloride was dissolved in distilled water, and sodium sulfate was added slowly to the solution and stirred homogeneously for 2 h. The final solution was moved to an autoclave for thermal treatment. Cadmium chloride was sulfurized during thermal treatment at 120 ºC for 12 h under a nitrogen environment. The resulting precipitate was washed with distilled water and then dried at 60 ºC for 24 h. The synthesized CdS powders with five weight ratios – 0.1, 0.5, 1.0, 5.0, and 10.0 wt % – were added to an ethanol solution containing nano-sized TiO_2 powder. The slurries were milled until the solvent had disappeared completely, and then the powder was thermally treated at 400 ºC for 1 h for stable cross linking between TiO_2 and CdS under nitrogen condition. These CdS/TiO_2 composites were used as a light scattering material in electrode of DSSC on the blocking layer of nano-sized TiO_2 film, and their photovoltaic performances were compared with that of DSSC-assembled by pure TiO_2/TiO_2 electrode.

The synthesized CdS powders were examined by X-ray diffraction (XRD; MPD, PANalytical) with nickel-filtered CuKα radiation (30 kV, 30 mA), and their shapes were measured by a transmission electron microscope (TEM; H-7600, Hitachi) operated at 120 kV. UV-visible spectra were obtained using a Cary 500 spectrometer with a reflectance sphere in the range of 200-800 nm. Photoluminescence (PL) spectroscopy was also performed to determine the number of photo-excited electron hole pairs using a PL mapping system (325 nm, LabRamHR, Jobin Yvon, at Korea Photonics Technology Institute Material Characterization Center).

Assembly of Doubled-Layered TiO_2/CdS-TiO_2-DSSCs. For preparation of the CdS-TiO_2 combined thin films for DSSCs, a paste was produced by mixing 2.0 g of TiO_2 (a commercial titanium dioxide, P-25 (anatase:rutile = 7:3), 20-70 nm, Degusa) or CdS-TiO_2 composite powders with a mixture consisting of 5.0 g of α-tepinol, 0.5 g of cellulose, and 20 mL of ethanol, after sonication for 24 h at 1200 Wcm^{-2}. The TiO_2 or CdS-TiO_2 composite film was fabricated by coating onto a fluorine-doped tin oxide (FTO) conducting glass plate (Hartford FTO, ~15 $ohmcm^{-2}$, 80% transmittance in visible region) using a squeeze printing technique. The film was treated by heating at 450 ºC for 30 minutes to remove the additives. For DSSC manufacture, the prepared thin film electrode was immersed in a 3.0×10^{-4} M N719 dye solution at room temperature for 2 h, rinsed with anhydrous ethanol and dried. A Pt-coated FTO electrode was placed over the dye-adsorbed TiO_2 or CdS-TiO_2 composite electrode, and the edges of the cell were sealed with a sealing sheet (PECHM-1, Mitsui-Dupont Polychemical). A redox electrolyte consisted of 0.5 mol KI, 0.05 mol I_2, and 0.5 mol 4-*tert*-butylpyridine was used as a solvent.

The photocurrent-voltage (I-V) curves were used to calculate the J_{sc}, V_{oc}, fill factor (FF), and overall conversion efficiency of the DSSCs. I-V curves were measured under white light irradiation from a xenon lamp (max. 150W) using a sun 2000 solar simulator (ABE technology). The light intensity was adjusted with a Si solar cell for approximated AM-1.5 radiation. The incident light intensity and active cell area were 100 $mWcm^{-2}$ (one sun illumination) and 0.25 cm^2 (0.5 × 0.5 cm), respectively. Impedance measurements were performed with the same condition of the DSSCs. The frequency range was between 0.1 and 100 kHz with an ac signal of 10 mV amplitude applied by a CompactStat electrochemical interface from IVIUM STAT technology. The applied bias voltage and ac amplitude were set at the V_{oc} of the DSSCs. The recombination property was measured by intensity modulated photovoltage spectroscopy (IMVS) using the same machine as used in the impedance measurement, with a red light-emitting diode (λ_{max} = 620 nm).

Results and Discussion

Physical Properties of Synthesized CdS. Figure 1(a) shows the crystallinity and photos obtained from the XRD pattern and SEM image of the CdS. All the reflection peaks of the different samples could be indexed to hexagonal CdS with lattice constants of α = 4.141 Å and c = 6.718 Å, which are in good agreement with the literature data (JCPDS card no. 41-1049). Compared with the standard card, the relative intensities of the peaks corresponding to the (100), (002), (101), (110), (103), and (112) planes are obvious; the (101) diffraction peaks in hexagonal CdS are usually strong and narrow,[1-4] however our sample had a higher (002) peak, which may be ascribed to the preferential growth along the (002) plane of the CdS crystallites. The mean crystalline size calculated using Scherrer's equation, $D = \kappa\lambda/\beta\cos\theta$., was

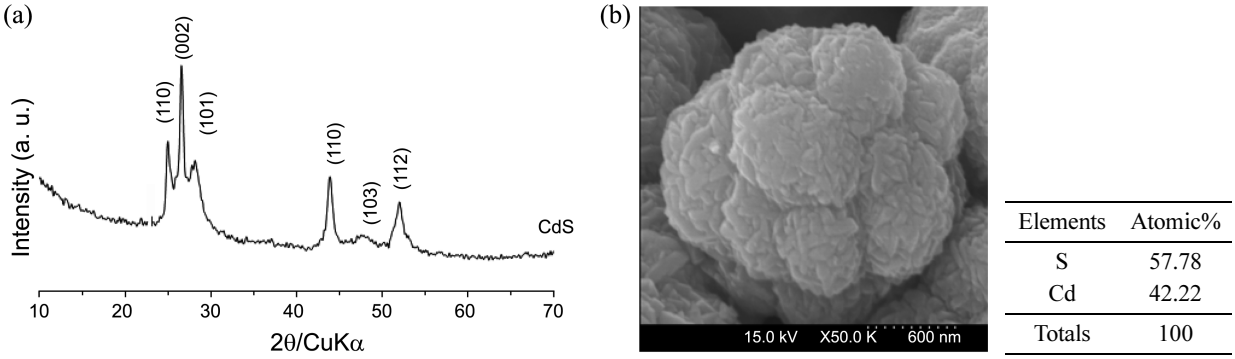

Elements	Atomic%
S	57.78
Cd	42.22
Totals	100

Figure 1. XRD patterns (a) and SEM images (b) of CdS prepared using a conventional hydrothermal method.

11.25 nm. The atomic composition was analyzed by energy dispersive X-ray spectroscopy (EDS) study, which revealed the presence of Cd and S as the only elementary components of the product of Cd:S at an atomic ratio = 42.22:57.78, which is close to the stoichiometric CdS. Figure 1(b) shows a high-magnification SEM image of the CdS. The nanorod-type CdS is the most common,[1-10] and the morphologies seem to be dependent on the type of additives and sulfur species. In this study, however, hollyhock-like particles with a width of 1.5-2.0 μm were obtained and were aggregated into hexagonal petal-shaped clumps of size 10 nm.

Figure 2(a) and (b) displays the UV-visible and PL spectrum of the synthesized CdS. Absorption spectroscopy is a good way to study any change in particle size with a small change in the chemical nature of the particle surface. A practical method is to equate energy gap with the wavelength at which the absorption is at point of the tangential part of the meeting extrapolation[17] or of that at the excitonic (shoulder) peak, called $\lambda_{1/2}$.[8] In our results, the sample had a steeper absorption edge, which is similar with the results obtained by the Tauc equation.[17] The absorption band of CdS for the hexagonal symmetry of Cd^{2+} normally appears at approximately 575 nm. Band gaps in semiconductor materials are closely related to the wavelength range absorbed, where the band gap decreases with increasing absorption wavelength. The absorption band gap energy can be determined by the following equation: $(\alpha h\nu)^n = B(h\nu\text{-}E_g)$, where hν is the photon energy, α the absorption coefficient, B a constant relative to the material and n a value that depends on the nature of transition (2 for a direct allowed transition, 2/3 for direct forbidden transition, and 1/2 for indirect allowed transition). The band gaps obtained by extrapolation in CdS (575 nm) were about 2.10 eV. As the semiconductor electrode plays the important roles of electron-receiving and -giving in DSSCs, and its light absorption is therefore important, the electron transfer is more crucial to enhance the DSSC performance, which indicates that the CdS effectively absorbs larger light ranges than pure TiO_2. The optical property of the hollyhock-like CdS was investigated by PL spectrum, as shown in Figure 2(b). The PL curve suggests that the electrons in the valence band were transferred to the conduction band, and that the excited electrons were then stabilized by photoemission. In general, it is very important that the PL intensity increases with the increasing number of emitted electrons resulting from recombination between excited electrons and holes, and, consequently, that the photo-activity decreases. The CdS nano-hollyhock particles featured three green emission bands and detailed analysis revealed that the green emission consisted of three strong emission bands centered at 530, 550 and 575 nm. Although the PL properties of CdS nano-crystals have been widely studied, those of CdS nanoparticles have not. Two studies[9,13] found that the weak infrared PL band arises from the electron transition from the surface states to the valence band of CdS nanorods. In our study, however, the band was not determined due to the deferent morphology of the hollyhock-like particles. The energy of 530, 550, and 575 nm (2.27, 2.20, and 2.10 eV) could be identified as the band gap or the band-to-band emission of bulk CdS, which has a band gap of 2.4 eV at room temperature.[13]

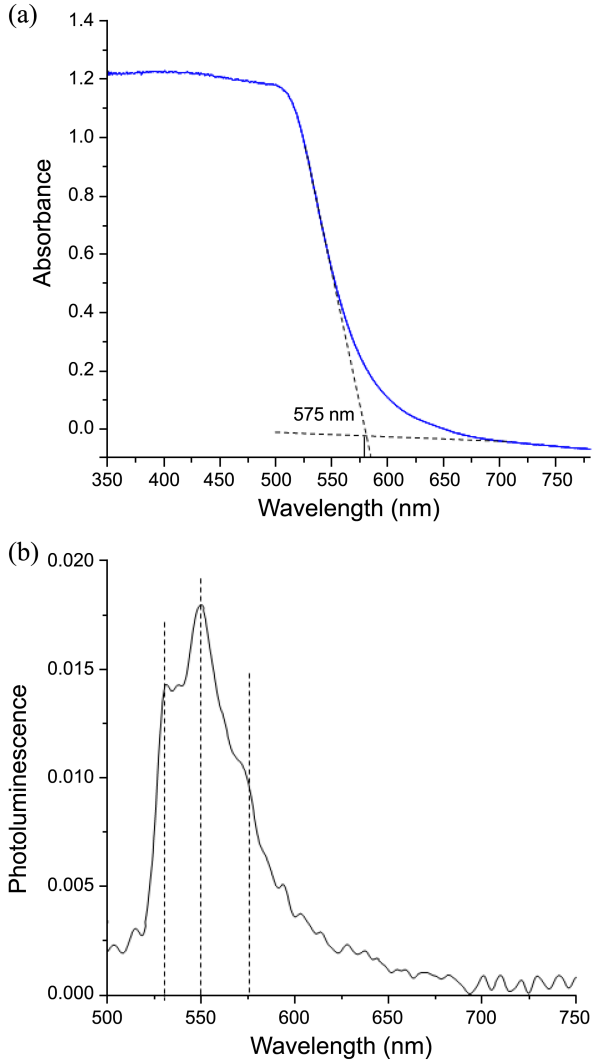

Figure 2. UV-visible (a) and photoluminescence (b) spectra of CdS.

Figure 3. shows the I-V curves and photovoltaic efficiencies of the DSSCs assembled with double-layered TiO_2/TiO_2 and TiO_2/CdS-TiO_2. The FF and solar energy conversion efficiency (η) were calculated according to Eqs. (1) and (2), respectively.

$$FF = I_{max} \times V_{max}/I_{sc} \times V_{oc}, \quad (1)$$

$$\eta\ (\%) = P_{out}/P_{in} \times 100 = I_{max} \times V_{max}/P_{in} \times 100 = I_{sc} \times V_{oc} \times FF. \quad (2)$$

The film thickness in the two DSSCs was 12 μm when coated with a double layer, in which the first and second coats act as the blocking and scattering layers, respectively. The power conversion efficiency was 4.25% in the DSSC consisting of a double-layered TiO_2 (blocking layer)/TiO_2 (scattering layer), with V_{oc} of 0.66 V and J_{sc} of 9.62 mA/cm^2. Both V_{oc} and J_{sc} increased in the double-layered TiO_2 (blocking layer)/CdS-TiO_2 (scattering layer)-DSSC. In parti-

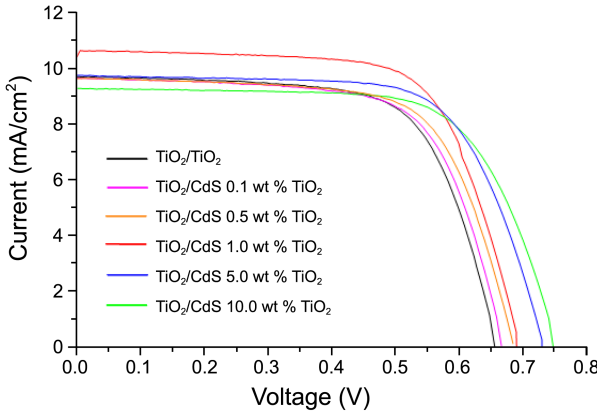

Sample	Voc	J_{sc} (mA/cm^2)	Fill factor	Efficiency (%)
TiO_2/TiO_2	0.6578	9.619	0.6710	4.25
TiO_2/CdS 0.1 wt % TiO_2	0.6675	9.512	0.6737	4.28
TiO_2/CdS 0.5 wt % TiO_2	0.6838	9.584	0.6647	4.38
TiO_2/CdS 1.0 wt % TiO_2	0.6907	10.64	0.6660	4.90
TiO_2/CdS 5.0 wt % TiO_2	0.7290	9.786	0.6650	4.74
TiO_2/CdS 10.0 wt % TiO_2	0.7474	9.324	0.6651	4.62

Figure 3. I-V curves of the DSSCs fabricated with double-layered TiO_2/TiO_2 and TiO_2/CdS-TiO_2.

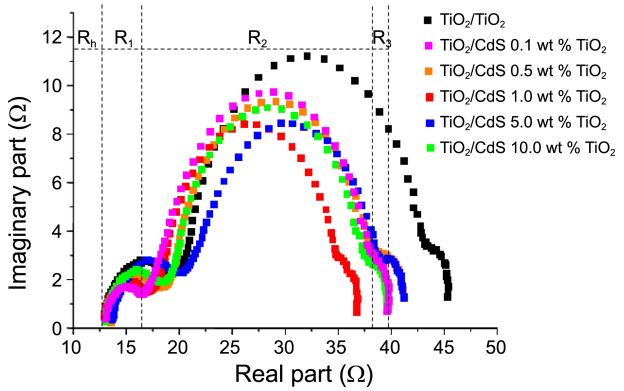

Figure 4. EIS of the DSSCs fabricated with double-layered TiO_2/TiO_2 and TiO_2/CdS-TiO_2.

Samples	Rh	R1	R2	R3
TiO_2/TiO_2	12.94	6.52	23.71	2.19
TiO_2/CdS 0.1 wt % TiO_2	12.98	3.58	22.30	1.11
TiO_2/CdS 0.5 wt % TiO_2	13.56	4.89	20.11	2.61
TiO_2/CdS 1.0 wt % TiO_2	12.92	4.18	18.08	1.67
TiO_2/CdS 5.0 wt % TiO_2	12.94	5.78	18.77	2.19
TiO_2/CdS 10.0 wt % TiO_2	13.70	6.34	19.28	1.93

cular, the voltage dramatically increased with an increase in the CdS photosensitizer content in the scattering layer. Therefore, the conversion efficiency was maximized at 4.90% in the TiO_2/1.0 wt % CdS-TiO_2-DSSC.

The impedance spectra shown in Figure 4 illustrated three semicircles in the measured frequency range of 0.1-100 kHz. The ohmic serial resistance (R_h) is associated with the series resistance of the electrolytes and electric contacts in the

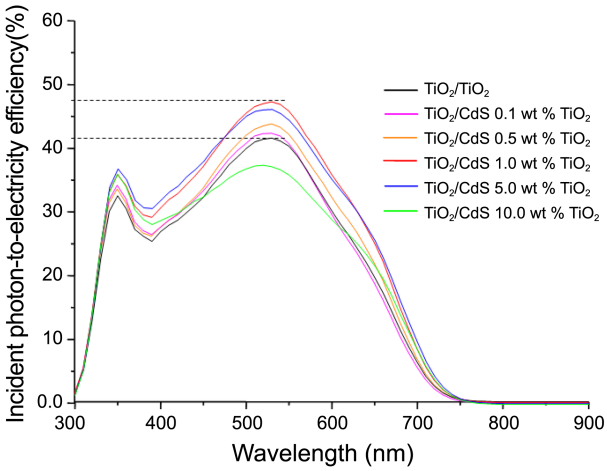

Figure 5. IPCE curves of the DSSCs fabricated with double-layered TiO_2/TiO_2 and TiO_2/CdS-TiO_2.

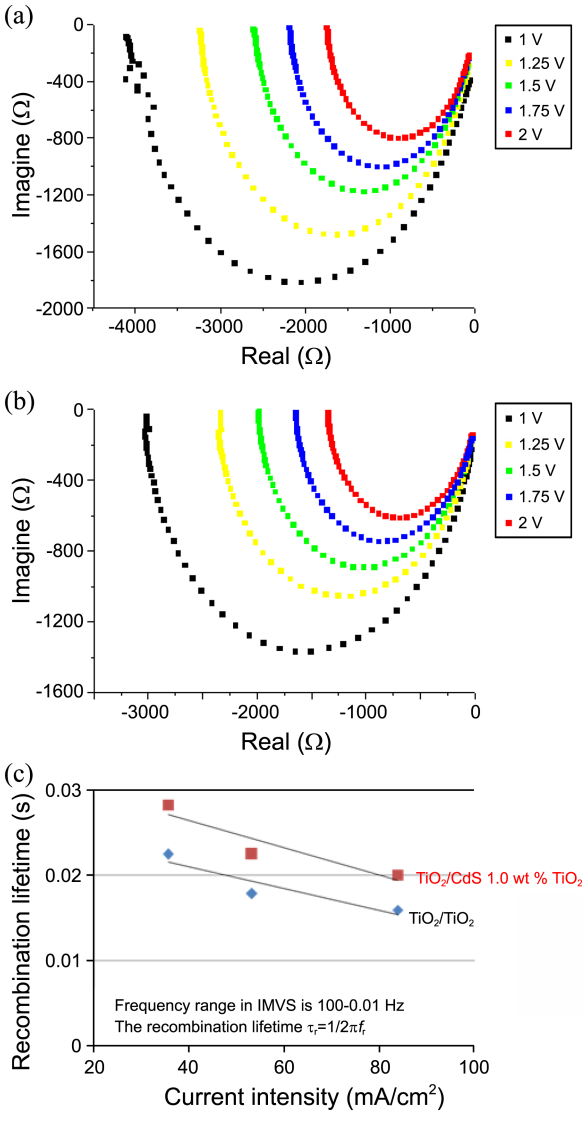

Figure 6. IMVS curves of the DSSCs fabricated with double-layered TiO_2/TiO_2 (a) and TiO_2/1.0 wt % CdS-TiO_2 (b), and the relation between recombination time and current intensity (c).

DSSCs. R_1, the charge transfer resistance, occurs at the Pt counter-electrode. R_2 has been associated with the resistance at the TiO_2 (semi-conducting electrode)/dye/electrolyte interface, whereas R_3 has been associated with the Nernstian diffusion within the electrolytes.[18] The TiO_2/TiO_2-DSSC appeared to have higher total resistances in the current path across the device than the TiO_2/CdS-TiO_2-DSSC. Notably, R_2 was largely decreased in the cell assembled with the TiO_2/1.0 wt % CdS-TiO_2-DSSC. This result revealed that electron transfer easily occurred over the CdS-TiO_2 composite surface, and thereby enhanced the photocurrent and powder efficiency of DSSCs.

The incident photon-to-electricity efficiency (IPCE) in Figure 5 indicates the number of incident photons inside the cell and their contribution to the efficiency.[19] DSSCs that primarily respond to the wavelength of visible light were measured in the region of 300-750 nm. The dye that reacted at a wavelength of 530-540 nm had the highest quantum number. The quantum efficiency was reduced from 48% for the DSSC assembled with the CdS-TiO_2 scattering layer to about 42% for those with the TiO_2 scattering layer. As a result, the quantum efficiency was increased to approximately 6%, which confirmed that the CdS scattering layer on the electrode induced more photons. Overall, the measured IPCE values were increased for all wavelengths within the studied range, and the wavelengths were shifted to longer ones.

Figure 6(a) and (b) shows typical IMVS response curves for the TiO_2/TiO_2- and TiO_2/1.0 wt % CdS-TiO_2-DSSC arrays, respectively. The IMVS plots display a semicircle in both DSSCs, and the circle of IMVS was shifted to the right in the TiO_2/1.0 wt % CdS-TiO_2-DSSC. The shift indicated that slower recombination could be expected in the oriented TiO_2/1.0 wt % CdS-TiO_2-DSSC than in the TiO_2/TiO_2-DSSC. Recombination in DSSCs was focused at two places: between the highest occupied molecular orbital (HOMO) and the lowest unoccupied molecular orbital (LUMO) of the dye first, and between the electrons in the semiconductor's conduction band and the hole of the valence band. In order to improve the DSSC performance, fast transition times must be combined with a slow recombination. The recombination time can be determined from $\tau_r = 1/2\pi f_r$, where f_r is the characteristic frequency minimum of the IMVS imaginary component,[20,21] and the relation is shown in Figure 6(c). The recombination time was increased with an increase in the approved current intensity; however, the rate was slower in the TiO_2/1.0 wt % CdS-TiO_2-DSSC than in the TiO_2/TiO_2-DSSC.

Conclusions

To enhance the solar energy conversion efficiency, CdS was prepared and coated with TiO_2 as a scattering material over a double-layered TiO_2/CdS-TiO_2 electrode. The TiO_2/CdS-TiO_2-DSSC showed better solar energy conversion efficiency than the double-layered TiO_2/TiO_2-DSSC electrode did. The efficiency of the TiO_2/1.0 wt % CdS-TiO_2-DSSC was approximately 4.90%, due to the slower recombination time. This result indicated that the CdS-TiO_2 electrode acts as a scattering layer of incident light path and that an increasing array of current density was obtained with more photons, which thus improved the quantum efficiency (IPCE).

Acknowledgments. This work was supported by the National Research Foundation of Korea (NRF) grant funded by the Korea government (MEST) (No. 2011-0003286), for which the authors are very grateful.

References

1. Ni, Y.; Ma, X.; Hong, J.; Xu, Z. *Mater. Lett.* **2004**, *58*, 2754.
2. Xia, Q.; Chen, X.; Zhao, K.; Liu, J. *Mater. Chem. Phys.* **2008**, *111*, 98.
3. Thongtem, T.; Phuruangrat, A.; Thongtem, S. *Mater. Lett.* **2007**, *61*, 3235.
4. Qingqing, W.; Gaoling, Z.; Gaorong, H. *Mater. Lett.* **2005**, *59*, 2625.
5. Li, C.; Yuan, J.; Han, B.; Shangguan, W. *Inter. J. Hydrogen Energy* **2011**, *36*, 4271.
6. Ghows, N.; Entezari, M. H. *Ultrasonics Sonochem.* **2011**, *18*, 629.
7. Thongtem, T.; Phuruangrat, A.; Thongtem, S. *Ceramics Inter.* **2009**, *35*, 2817.
8. Zhong, S.; Zhang, L.; Huang, Z.; Wang, S. *Appl. Surf. Sci.* **2011**, *257*, 2599.
9. Maurya, A.; Chauhan, P. *Mater. Chracterization* **2011**, *62*, 382.
10. Qingqing, W.; Gang, X.; Gaorong, H. *J. Solid State Chem.* **2005**, *178*, 2680.
11. Niitsoo, O.; Sarkar, S. K.; Pejoux, C.; Rühle, S.; Cahen, D.; Hodes, G. *J. Photochem. Photobiol. A: Chem.* **2006**, *181*, 306.
12. Zhu, Q.; Chen, J.; Xu, M.; Tian, S.; Pan, H.; Qian, J.; Zhou, X. *Solid State Sci.* **2011**, *13*, 1299.
13. Jiang, X.; Chen, F.; Qiu, W.; Yan, Q.; Nan, Y.; Xu, H.; Yang, L.; Chen, H. *Sol. Energy Mater. Sol. Cells* **2011**, *94*, 2223.
14. Prabakar, K.; Seo, H.; Son, M.; Kim, H. *Mater. Chem. Phys.* **2009**, *117*, 26.
15. Lee, J.-K.; Jeong, B.-H.; Jang, S.-I.; Kim, Y.-G.; Jang, Y.-W.; Lee, S.-B.; Kim, M.-R. *J. Ind. Eng. Chem.* **2009**, *15*, 724.
16. Kim, G.-O.; Kim, K.-W.; Cho, K.-K.; Ryu, K.-S. *Appl. Chem. Eng.* **2011**, *22*, 190.
17. Xiao, J.; Li, Y.; Jiang, A. *J. Mater. Sci., Technol.* **2011**, *27*, 403.
18. Chae, J.; Kang, M. *J. Power Sources* **2011**, *196*, 4143.
19. Park, N. G.; Schlichthorl, G.; can de Lagemaat, J.; Cheong, H. M.; Mascarenhas, A.; Frank, A. J. *J. Phys. Chem. B* **1999**, *103*, 3308.
20. Franco, G.; Gehring, J.; Peter, L. M.; Ponomarev, E. A.; Uhlendorf, I. *J. Phys. Chem. B* **1999**, *103*, 692.
21. Schlichthorl, G.; Park, N. G.; Frank, A. J. *J. Phys. Chem. B* **1999**, *103*, 782.